Mapping the immunogenic landscape of near-native HIV-1 envelope trimers in non-human primates

Christopher A. Cottrell[1,2,3], Jelle van Schooten[4], Charles A. Bowman[1], Meng Yuan[1], David Oyen[1], Mia Shin[1], Robert Morpurgo[4], Patricia van der Woude[4], Marielle van Breemen[4], Jonathan L. Torres[1], Raj Patel[1], Justin Gross[1], Leigh M. Sewall[1], Jeffrey Copps[1], Gabriel Ozorowski[1,2,3], Bartek Nogal[1,2,3], Devin Sok[2,3,5], Eva G. Rakasz[6], Celia Labranche[7], Vladimir Vigdorovich[12], Scott Christley[13], Diane G. Carnathan[3,14], D. Noah Sather[12], David Montefiori[7,8], Guido Silvestri[3,14], Dennis R. Burton[2,3,5,9], John P. Moore[10], Ian A. Wilson[1,2,3,11], Rogier W. Sanders[1,10,#], Andrew B. Ward[1,2,3,#], Marit J. van Gils[4,#]

[1]Department of Integrative Structural and Computational Biology, The Scripps Research Institute, La Jolla, CA 92037, USA.

[2]IAVI Neutralizing Antibody Center, The Scripps Research Institute, La Jolla, CA 92037, USA.

[3]Consortium for HIV/AIDS Vaccine Development, The Scripps Research Institute, La Jolla, CA 92037, USA.

[4]Department of Medical Microbiology, Amsterdam UMC, University of Amsterdam, 1105 AZ Amsterdam, The Netherlands.

[5]Department of Immunology and Microbiology, The Scripps Research Institute, La Jolla, CA 92037, USA.

[6]Wisconsin National Primate Research Center, University of Wisconsin, Madison, WI 53715, USA.

[7]Department of Surgery, Duke University Medical Center, Durham, NC 27710, USA.

[8]Duke Human Vaccine Institute, Duke University Medical Center, Durham, NC 27710, USA.

23 [9]The Ragon Institute of Massachusetts General Hospital, Massachusetts Institute of Technology
24 and Harvard University, Cambridge, MA 02139, USA.
25 [10]Department of Microbiology and Immunology, Weill Medical College of Cornell University, New
26 York, NY 10021,USA
27 [11]The Skaggs Institute for Chemical Biology, The Scripps Institute, La Jolla, CA 92037, USA
28 [12]Center for Global Infectious Disease Research, Seattle Children's Research Institute, Seattle, WA
29 98109, USA.
30 [13]Department of Population and Data Sciences, UT Southwestern Medical Center, Dallas, TX
31 75390, USA
32 [14]Yerkes National Primate Research Center, Emory University, Atlanta, GA 30322, USA;
33 [#]corresponding author; m.j.vangils@amc.uva.nl; andrew@scripps.edu; r.w.sanders@amc.uva.nl

Abstract

The induction of broad and potent immunity by vaccines is the key focus of research efforts aimed at protecting against HIV-1 infection. Soluble native-like HIV-1 envelope glycoproteins have shown promise as vaccine candidates as they can induce potent autologous neutralizing responses in rabbits and non-human primates. In this study, monoclonal antibodies were isolated and characterized from rhesus macaques immunized with the BG505 SOSIP.664 trimer to better understand vaccine-induced antibody responses. Our studies reveal a diverse landscape of antibodies recognizing immunodominant strain-specific epitopes and non-neutralizing neo-epitopes. Additionally, we isolated a subset of mAbs against an epitope cluster at the gp120-gp41 interface that recognize the highly conserved fusion peptide and the glycan at position 88 and have characteristics akin to several human-derived broadly neutralizing antibodies.

46 **Introduction**

47 HIV-1 continues to cause significant morbidity and mortality around the world with an estimated
48 1.7 million new infections in 2018[1], which emphasizes the need for an effective prophylactic
49 vaccine. The HIV-1 envelope glycoprotein (Env) is the sole target for neutralizing antibody (NAb)
50 responses. Studies of infected patients have led to the isolation of NAbs against multiple different
51 epitopes on the Env surface that are capable of both neutralizing most circulating strains and
52 providing passive protection against repeated viral challenges in non-human primates (NHPs)[2-5].
53 Extensive research efforts, including structure-based engineering of Env immunogens, are
54 currently directed towards developing vaccine strategies to successfully elicit broadly
55 neutralizing antibodies (bNAbs) against specific Env epitopes[6-12]. The development and structural
56 determination of soluble native-like Env trimer mimics, particularly ones based on the SOSIP
57 technology, has provided a platform for structure-based immunogen design[13-16]. NAbs induced
58 by SOSIP trimers in NHPs can protect against challenge with an autologous Simian-Human
59 Immunodeficiency virus (SHIV)[17,18]. However, as NAbs with the required breadth of activity have
60 not yet been induced in trimer-immunized animals, improvements to current vaccine design and
61 delivery strategies are clearly needed.

62 Characterizing the antibody response to SOSIP trimers may provide useful information for
63 guiding immunogen design. Initial analyses of rabbits immunized with BG505 SOSIP.664 trimers,
64 including studies of isolated monoclonal antibodies (mAbs), showed that autologous NAbs
65 targeted a large hole in the glycan shield of the BG505 virus caused by the absence of
66 glycosylation sites at positions 241 and 289[19,20]. The 241 glycan is highly conserved (97%) among
67 HIV-1 strains and while the 289 glycan is less conserved, it is still present in 79% of viruses. The

68 required absence of typically conserved glycans explains why the NAbs isolated from the trimer-
69 immunized rabbits lack breadth[19]. Later studies involving BG505 trimer-immunized rabbits,
70 guinea pigs, and NHPs have identified additional narrow-specificity neutralizing serum responses
71 that recognize epitopes in the C3/V4, C3/V5, and V1 regions, with mAbs isolated from guinea pigs
72 targeting the C3/V4 epitope[17,20-23].

73 Here, we describe a detailed characterization of neutralizing and non-neutralizing mAbs
74 isolated from two rhesus macaques (RMs) previously immunized with the BG505 SOSIP.664
75 trimer [24]. We identified multiple mAbs targeting the 289-glycan hole on the BG505 SOSIP.664
76 trimer or a neo-epitope cluster at the base of the trimer. The most potent NAb isolated targeted
77 the gp120/gp41 interface at an epitope that significantly overlaps with the epitope of human
78 bNAb VRC34[25]. Insights from the induction of these NAbs through vaccination can be further used
79 to develop immunogens and immunization strategies to induce cross-reactive antibody
80 responses.

81

82 **Results**

83 **Indian origin rhesus macaque BCR germline database**

84 The majority of bNAbs isolated from HIV-infected patients have exceedingly high levels of
85 somatic hypermutation (SHM)[5,26]. Accurately measuring levels of SHM elicited during
86 immunization experiments is a critical component to ensuring the elicited antibodies are
87 acquiring the level of mutations associated with neutralization breadth. To accurately measure
88 the extent of SHM, the mAb sequences that we obtained from BG505 SOSIP.664 trimer-
89 immunized RMs required comparison to a germline B-cell receptor (BCR) reference database.
90 The IMGT reference database for RMs is incomplete and contains a mixture of genes/alleles from
91 both Chinese and Indian origin animals. Given the high levels of genetic diversity in the
92 Immunoglobulin (Ig) loci among RMs from different origins[27] and the general use of Indian origin
93 RMs in most HIV-1 immunization experiments conducted in the United States, we constructed a
94 germline database containing gene/alleles from only Indian origin RMs. The gene/alleles from
95 the published database[28] were aligned to the Mmul_8.0.1 Indian origin RM genome assembly
96 using BLAST[29,30]. Sequences that were not identical to the reference genome were eliminated.
97 Additional genes/alleles from publicly available Indian origin RM genomic DNA sequencing
98 datasets[21,31] were added to the database. After duplicates were removed, the resulting new
99 database contained 189 IGHV, 70 IGHD, 9 IGHJ, 188 IGKV, 5 IGKJ, 147 IGLV, and 13 IGLJ
100 genes/alleles (Table S1).

101 Recent advances in BCR repertoire sequencing and analysis have enabled the use of next-
102 generation sequencing (NGS) datasets for inferring novel genes/alleles[27,32,33]. Using the database
103 described above as an initial database, we performed IgDiscover analysis[27] on IgM BCR sequences

104 derived from five Indian origin RMs. Additionally, we performed IgDiscover analysis on previously
105 obtained Indian origin RM BCR NGS datasets that were downloaded from the NCBI sequence read
106 archive[27,34] or obtained directly from the study authors[28]. Inferred genes/alleles were kept if they
107 were detected in more than one animal or if they were identical to RM genes/alleles that were
108 previously deposited in the NCBI database. We added 113 IGHV, 18 IGKV, and 18 IGLV
109 genes/alleles to our germline database (http://ward.scripps.edu/gld/) resulting in a total of 302
110 IGHV, 206 IGKV, and 165 IGLV genes/alleles. This updated database was then converted into a
111 custom IgBLAST database and subsequently used to analyze our BG505-specific mAbs sequences
112 with IgBLAST[35].
113
114 **Antigen-specific mAbs isolated from BG505 SOSIP.664 trimer-immunized RMs**
115 To better understand the immunogenicity of the BG505 SOSIP.664 trimers in previously
116 immunized Indian origin RMs[24] we selected the two animals (rh1987 and rh2011) with the highest
117 serum neutralization activity against the autologous BG505.T332N pseudovirus for in-depth mAb
118 analysis. Peripheral blood mononuclear cells (PBMCs) from the following time points were
119 selected for BG505 SOSIP.664 trimer-specific IgG-positive single memory B-cell sorting: (i) two
120 weeks prior to the fourth immunization (week 22), (ii) 1 week after the fourth immunization
121 (week 25) and (iii) 1 week after the sixth immunization (week 53) (Fig 1A). In total, 25 and 17
122 mAbs were cloned from RMs rh1987 and rh2011, respectively (Fig 1B).
123 The BG505-specific mAb sequences were analysed using our germline database and
124 shown to be evenly distributed between kappa and lambda light chains (KC and LC) usage (Fig
125 1B). For animal rh1987, 11 KC and 14 LC mAbs were isolated. Their average heavy chain (HC) SHM

126 (nucleotide level) was 6.4% (range: 2.1%-10.2%) with an average HC complementarity-
127 determining region 3 (CDR-H3) length of 15 amino acids (aa) (range: 7-23) (Table S2). The rh1987
128 KC mAbs utilized HC variable genes from the IGHV3 and IGHV4 families and predominantly used
129 KC V genes from the IGKV1 family (Table S2). All of the rh1987 KC mAbs had a CDR-L3 length of 9
130 aa and their average KC SHM (nucleotide level) was 4.7% (range: 2.6%-6.0%) (Table S2). A single
131 clonal family with 4 members (RM19A) was detected among rh1987 KC mAbs with members
132 isolated from both week 22 and week 25 samples (Table S2). The rh1987 LC mAbs used HC V
133 genes from the IGHV1, IGHV3 and IGHV4 families and LC V genes mainly from the IGLV2 gene
134 family (Table S2). The rh1987 LC mAbs had an average CDR-L3 length of 10 aa (range: 9-11) with
135 an average LC SHM (nucleotide level) of 3.8% (range: 0.9%-10.6%) (Table S2). Two clonal families
136 (RM19B [2 members] and RM19C [4 members]) were identified among the rh1987 LC mAbs
137 isolated from weeks 22 and 25 (Table S2).

138 For animal rh2011, 8 KC and 9 LC mAbs were isolated. Their average HC SHM rate
139 (nucleotide level) was 6.1% (range: 3.0%-9.1%) and they had an average CDR-H3 length of 17 aa
140 (range 10-20) (Table S2). Half of the rh2011 KC mAbs belonged to the RM20E clonal family,
141 isolated from the week 53 sample. The RM20E clonal family utilized the HC V gene IGHV5-
142 ABI*01_S2502 and the KC V gene LJI.Rh_IGKV2.71 (Table S2). Overall, the rh2011 KC mAbs had
143 an average KC SHM rate (nucleotide level) of 4.1% (range: 3.0%-5.3%) and a CDR-L3 length of 9
144 aa (Table S2). Among the rh2011 LC mAbs, two clonal families (RM20A [4 members] and RM20B
145 [2 members]) were isolated from weeks 22 and 25 samples (Table S2). Overall, the rh2011 mAbs
146 had an average LC SHM rate (nucleotide level) of 4.4% (range: 2.1%-6.4%) and an average CDR
147 L3 length of 10.6 aa (range: 9-11) (Table S2).

148

149 **BG505-specific mAbs recognize multiple Env regions**

150 All 42 mAbs bound to the BG505 SOSIP.664 trimer in ELISA, but only 11 of the 25 mAbs from
151 rh1987 and 9 of the 17 from rh2011 bound the corresponding gp120 monomer (Fig S1). The mAbs
152 were tested for neutralization activity against the autologous BG505 clade A Tier 2 virus, its
153 glycan-611 knockout variant (N611A), and the heterologous SF162 clade B Tier 1A virus. Only a
154 few mAbs, 4 from rh1987 and 2 from rh2011, neutralized the BG505.T332N pseudovirus but one
155 of them, RM20F from rh2011, did so potently (Fig 1C). Two mAbs from rh1987 and 4 from rh2011
156 were able to potently neutralize the N611A-variant despite lacking activity against the autologous
157 BG505.T332N pseudovirus (Fig 1C and D). None of the 42 mAbs neutralized the easy-to-neutralize
158 heterologous SF162 virus (Fig 1C and D).

159

160 **EM-based epitope mapping revealed mAbs isolated from both animals target 4 distinct, but**
161 **somewhat overlapping epitopes**

162 We used low resolution, negative stain, single particle electron microscopy (EM) to visualize
163 where a representative subset of the isolated mAbs bound on the surface of the BG505 SOSIP
164 trimer. The majority (55%) of mAbs isolated were non-neutralizing antibodies that bound to the
165 base of the BG505 SOSIP trimer (Figs 2A, S2, and Table S2) at a neo-epitope cluster that is
166 occluded by the viral membrane on HIV-1 virions. Fabs bound to the base of the soluble trimer
167 via multiple angles of approach and utilized a variety of heavy and light chain genes/alleles to do
168 so (Fig 2A and Table S2). The extent of SHM in the base-targeting mAbs ranged from 2-10% in the
169 HC and 1-11% in the light chain (Table S2). Previous studies examining the polyclonal antibody

170 responses elicited by the BG505 SOSIP trimers in rabbits and RMs have shown that epitopes at
171 the base of the soluble trimer were targeted in every single animal analyzed [21,23,36]. Taken
172 together with our new data, it is clear that the base of SOSIP trimers contain an immunodominant
173 non-neutralizing neo-epitope cluster that is easily targeted by a variety of precursor BCRs in
174 different species.

175 A subset of mAbs from both animals bound to an epitope near the N611 glycan (Figs 2B
176 and S2). These mAbs were not capable of neutralizing the autologous BG505.T332N pseudovirus
177 but neutralized the BG505 N611A variant (Fig 1C and D). Two additional mAbs isolated from
178 rh2011 (RM20F and RM20H) bound to an epitope near the fusion peptide (FP) and were capable
179 of neutralizing both the autologous and N611A BG505 pseudoviruses, but the latter virus more
180 potently (Figs 2C and S2). MAbs from both animals targeted the 289-glycan hole epitope on
181 BG505, with some, isolated from rh1987, showing weak neutralization of the autologous
182 BG505.T332N pseudovirus (Figs 1C and 2D; Table S2). Multiple germline genes/alleles were used
183 to target the same 289-glycan hole epitope (Table S2).

184 To further assess the epitopes targeted following immunization with the BG505
185 SOSIP.664 trimer and verify that we isolated mAbs representative of the full serum antibody
186 response, we performed electron microscopy polyclonal epitope mapping (EMPEM)[36] using week
187 28 serum. EMPEM revealed that similar epitopes were targeted in both animals and that the
188 epitope assignments correlated well with the epitopes ascribed to mAbs generated by antigen-
189 specific B-cell sorting (Fig 2E versus S2).

190 A previous analysis of purified serum IgGs from RMs rh1987 and rh2011 identified the
191 C3/V5 epitope as a major target for neutralization activity[20]; however, none of the mAbs isolated

192 here targeted the C3/V5 epitope nor were they detected by EMPEM. While low resolution,
193 negative stain EM provides valuable information on where mAbs bind on the surface of HIV-1
194 Env, the molecular detail necessary to guide structure-based immunogen design requires high-
195 resolution structural data obtained by cryoEM and x-ray crystallography. We therefore selected
196 three Fabs (RM20J, RM20F, and RM20E1) that bound to different epitopes for high-resolution
197 structural determination.
198
199 **MAb RM20J binds to the α2 helix of gp120 and exploits a hole in the glycan shield of BG505 at**
200 **position 289**
201 We solved a 2.3 Å crystal structure of unliganded RM20J Fab and a 3.9 Å cryoEM structure
202 of RM20J Fab bound to the BG505 SOSIP Env trimer (Figs 3A and S3; Tables S4 and S5.). Together
203 these structures revealed the RM20J Fab binds to an epitope on a single gp120 protomer with
204 982 $Å^2$ of buried surface area (BSA). The CDR-H1 and CDR-H2 make contact with the C2 region of
205 gp120 including residues N289 and T290 (Fig 3B). A glycan at position N289 would directly clash
206 with both the CDR-H1 and CDR-H2 of RM20J (Fig 3B). CDR-L2 makes contact with the first N-
207 acetyl glucosamine sugar of the N355 glycan (Fig 3C). Additional contacts are made to the α2
208 helix of gp120 by RM20J CDR-H3 and CDR-L2 (Fig 3C). When compared to 10A, a previously
209 characterized 241/289 glycan hole targeting NAb isolated from a BG505 SOSIP.664-immunized
210 rabbit[19,36], RM20J binds to an epitope biased more towards 289 and away from 241 in the
211 241/289 glycan hole, revealing subtle differences in the recognition of the epitope (Figs 3D and
212 3E). Despite binding to the BG505 SOSIP trimer with high affinity (Table S3), RM20J was not able
213 to neutralize the autologous BG505.T332N pseudovirus (Fig 1C). Although the hypervariable

214 region of V4 was not resolved in the trimer structure, it lies directly above the RM20J epitope
215 and contains two additional glycans (N406 and N411) that may affect RM20J binding.
216 Comparisons between the glycosylation profiles of the BG505 viral Env and the SOSIP.664 trimer
217 revealed differences in the glycoforms present at positions N355, N406, and N411[37,38] with more
218 complex glycans being found on the viral Env that could hinder the ability of RM20J to bind on
219 the surface of the virus and, therefore, render it incapable of neutralization. Several of the mAbs
220 isolated from rh1987, including the RM19A clonal family, bind to a similar epitope as RM20J (Fig
221 2D, Fig S2, Table S2) and either fail to neutralize the autologous BG505 virus or do so with weak
222 potency (Fig 1C and D).
223
224 **MAb RM20F binds to a quaternary epitope at the gp120/gp41 interface that includes elements**
225 **of the fusion peptide and the N88 glycan**
226 For a more detailed view of the mode of RM20F recognition, we solved a 2.2 Å crystal
227 structure of unliganded RM20F Fab and a 4.3 Å cryoEM structure of RM20F Fab bound to BG505
228 SOSIP trimer (Figs 4A and S3; Tables S4 and S5). RM20F recognizes an epitope spanning two gp41
229 protomers and a single gp120 protomer that has 1126 Å² of BSA at the interface. The RM20F LC
230 contributes 22% of the paratope surface area (250 Å²) and makes contact with the poorly
231 conserved residues H85 (8.1% prevalence among global strains) and K229 (12.5% prevalence) in
232 the C1 and C2 regions of gp120 respectively (Fig 4B). The RM20F HC contributes the remaining
233 78% of the paratope surface area (876 Å²) and uses its 20 residue CDR-H3 to wedge between the
234 FP of the primary gp41 protomer and the HR2 helix of the adjacent gp41 protomer (Fig 4C).
235 Additional contacts with the fusion peptide proximal region (FPPR) of the primary gp41 protomer

236 are made by residues at the tip of CDR-H2 (Fig 4B). The N88 glycan accounts for 18% (198 Å²) of
237 the epitope BSA and makes contact with the CDR-H2 and FR-H3 regions of RM20F (Fig 4B). The
238 lack of connecting density, even at lower contour, between RM20F and the glycans at N611 and
239 N637 suggests these glycans do not substantially contribute to the epitope. Epitope mapping
240 using BG505.T332N mutant pseudoviruses showed that knocking out the N611 glycan (N611Q
241 mutant) substantially enhanced neutralization by RM20F, while knocking out the N637 glycan
242 (N637Q mutant) had no effect. (Fig 4D). Other virus mutants revealed that neutralization by
243 RM20F was sensitive to various sequence changes within the epitope, particularly at residues
244 H85 and E647 (84.3% prevalence) and N88 (N88 glycan knock out) (Fig 4D). The N88 glycan knock
245 out and the H85A mutation (to a lesser extent) significantly reduced neutralization activity of the
246 FP-targeting bNAb VRC34, but no effect on the CD4 binding site targeting bNAb VRC01 (Fig 4D).
247 Introducing the 241 or 289 glycans (S241N and P291T, respectively) modestly reduced the
248 neutralization activity of RM20F (Fig 4D). In comparison to the FP-targeting bNAbs VRC34 and
249 ACS202, RM20F lacked neutralization breadth when tested against a panel that included multiple
250 heterologous viruses (Fig S4) likely due to the dependency on poorly conserved residues.
251
252 **MAb RM20E1 binds to the fusion peptide and makes contact with two adjacent protomers**
253 We solved a 2.3 Å crystal structure of the unliganded RM20E1 Fab and 4.4 Å cryoEM
254 structure of RM20E1 Fab bound to BG505 SOSIP trimer and Fab PGT122 (Figs 5A and S3; Tables
255 S4 and S5). RM20E1 binds to an epitope composed of one gp120 and two gp41 protomers with
256 1178 Å² of BSA. Residues 515 to 520 of the FP in the primary gp41 protomer are sandwiched
257 between CDR-H3, CDR-L1, and CDR-L3 of RM20E1 (Fig 5B). CDR-H3 and FR-H1 make contact with

258 HR2 in the adjacent gp41 protomer (Fig 5C). Additionally, the FR-H1 makes contact near the
259 N611-glycan site in the adjacent gp41 protomer, but we observed no connecting density that
260 could be attributed to the N611-glycan itself (Fig 5C). RM20E1 avoids the N88 glycan but does
261 interact with residues in the C1 region of gp120, including H85, via its CDR-L1 (Fig 5B). Despite
262 recognition of the conserved FP, RM20E1 did not neutralize the autologous BG505.T332N
263 pseudovirus. The antibody did however potently neutralize the N611A glycan KO BG505
264 pseudovirus (Fig 1C) suggesting the epitope is shielded by the N611 glycan. The epitopes of the
265 FP-targeting bNAbs VRC34, ACS202, and DFPH-a.15 overlap to a large extent with the epitopes
266 of RM20E1 and RM20F (Fig 5D), with DFPH-a.15 and VRC34 also neutralizing more potently in
267 the absence of the N611 glycan[9,25,39,40]. The RM20E1-bound FP conformation is similar to the FP
268 conformation when bound by the bNAb VRC34 (Fig S5); however, the inability of RM20E1 to
269 accommodate the N611 glycan likely results in the lack of neutralization of the wild-type virus.
270

271 **Discussion**

272 A major goal of HIV-1 vaccine research is to elicit bNAbs able to neutralize the large
273 diversity of circulating HIV-1 strains in humans. However, how to achieve this goal remains a
274 critical problem. Native-like Env trimers are an important design platform for engineering
275 immunogens for bNAb induction[7-13,41,42]. BG505 SOSIP trimers were able to induce responses in
276 immunized RMs that potently neutralized the autologous Tier 2 virus[17,24]. When present at
277 sufficient titers, those NAbs protected against BG505-SHIV challenge[18]. Evaluating SOSIP trimers
278 in RMs can yield valuable information because of the close genetic relationship between RMs
279 and humans. Here, we isolated mAbs from two BG505 SOSIP.664 trimer-immunized RMs to

280 better understand how the immune system recognizes the trimers and the epitopes associated
281 with the potent, but limited, HIV-1 Tier 2 neutralization.

282 By mapping the epitopes of all of the mAbs isolated from the immunized RMs, rather than
283 focusing only on NAbs, we were able to identify several non-neutralizing and potentially
284 immunodominant epitopes that would ideally be eliminated in future immunization studies. As
285 shown previously with mAbs from rabbits immunized with BG505 SOSIP.664 trimers[19], the lack
286 of glycans at positions 241 and 289 in BG505 creates a large glycan hole which is targeted by
287 mAbs from both RMs. The mAbs isolated from RMs that target the 241/289 glycan hole are more
288 biased towards the 289-site compared to the previously characterized rabbit mAbs. This
289 difference may be attributed to the underlying differences in BCR repertoires between the two
290 animal models. In addition to the lack of glycans due to missing sequons that encode for
291 glycosylation, the recombinant BG505 SOSIP.664 trimer may also contain missing glycans even
292 when the correct sequon is present as previously observed by mass spectrometry studies of
293 glycopeptides[37,43]. Our study identified gp120/gp41 interface antibodies whose neutralization
294 was enhanced in the absence of the N611 glycan, suggesting that the BG505 SOSIP.664 trimer
295 may have sub-stoichiometric glycan occupancy in gp41 at this position, creating an unexpected
296 but immunogenic glycan hole. The elicitation of FP targeting mAbs in RMs with the BG505
297 SOSIP.664 trimer provides evidence that the FP bNAb epitope is accessible and immunogenic on
298 soluble Env trimer immunogens. Recent studies in mice, guinea pigs and RMs using synthetically
299 produced HIV fusion peptides covalently attached to carrier proteins as priming immunogens
300 followed by boosts with soluble Env trimer immunogens have also elicited FP specific antibodies
301 including some mAbs with neutralization breadth[9,44,45]. However, the majority of the animals

302 immunized in these studies do not develop neutralization breadth and instead develop potent
303 neutralization against the BG505 pseudovirus with the N611 glycan KO[9,44,45]. Given the
304 consistency across studies and animal models in eliciting potent NAbs that target the FP epitope
305 and require the absence of the N611 glycan, investing in strategies to quantify and enhance the
306 N611 glycan occupancy in soluble Env trimer immunogens, particularly for boost immunogens,
307 may improve the neutralization breadth elicited by FP-targeting immunization protocols.

308 The sorting probe used to isolate BG505 Env-specific B-cells was a C-terminally
309 biotinylated BG505 SOSIP.664 trimer bound to a fluorescent streptavidin tetramer. Steric
310 constraints between the base of the trimer and the streptavidin tetramer likely resulted in a
311 lower recovery of base epitope-specific B-cells. Despite this potential selection bias, 55% of the
312 mAbs isolated from the two immunized RMs bound to the base of the BG505 SOSIP.664 trimer,
313 indicating the base of the soluble trimer is the major target for antibody responses during
314 immunization. To reduce the immunogenicity of this epitope, glycans can be introduced to shield
315 this site or the native-like trimers could be constructed onto scaffolds or particles[46-49].

316 We were unable to construct individual germline BCR databases from RMs rh1987 and
317 rh2011 to precisely determine the SHM and gene/alleles usage as additional PBMC samples were
318 no longer available. Instead, we constructed a germline database containing BCR gene/alleles
319 from multiple Indian origin RMs that allowed us to measure SHM levels in the mAbs we isolated
320 from RMs. The new database provides web-based access (http://ward.scripps.edu/gld/) to a
321 curated and highly annotated general resource for examining BCR gene/alleles from Indian origin
322 RMs. Previous estimates of average SHM rates in mAb sequences from Env-immunized RMs were
323 8.9% and 6.1% for the HC and LC, respectively [50]. These apparently high levels of SHM following

324 repeated immunization with the exact same soluble Env immunogens were likely due to missing
325 germline gene/alleles from the database used to calculated SHM. Using the germline database
326 reported in this study, we were able to assign vaccine-elicited antibody sequences to specific
327 germline genes/alleles and determine levels of SHM much more accurately. The average levels
328 of SHM reported in this study (6.3% for HC and 4.2% for LC) are comparable to the average levels
329 of SHM reported in similar immunization studies where per animal germline BCR databases were
330 inferred using IgDiscover [51,52]. Our germline database provides a resource for assigning germline
331 genes/alleles and accurately calculating rates of SHM when inferring individual germline
332 databases for each animal is logistically impractical.

333 In conclusion, in this study, neutralizing and non-neutralizing mAbs with distinctive
334 epitopes were isolated and characterized in BG505 SOSIP.664-immunized RMs. We
335 demonstrated that a polyclonal response was elicited in two different RMs that target the BG505
336 SOSIP.664 trimer in highly similar ways. While rabbit antibody responses are dominated by the
337 base and 241-glycan hole epitopes, the RM mAbs target more diverse epitopes with mAbs also
338 targeting the FP and gp120/gp41 interface. The mAbs characterized here also provide a valuable
339 resource for epitope mapping and comparison to a wide array of BG505-based immunization
340 experiments, including the recently initiated BG505 SOSIP.664 human clinical trial
341 (NCT03699241). Finally, the FP-targeting mAbs in particular provide a structure-guided
342 opportunity to modify BG505 SOSIP and other trimers to focus the antibody response on the FP-
343 region, with the goal of eliciting bNAb-like antibodies.

344

345 **Methods**

346 **Immunizations of rhesus macaques**

347 Immunization samples used in this study were obtained from previously immunized RMs
348 described in Sanders et al. 2015 [24]. Briefly, RMs were immunized intramuscularly (i.m.) with 100
349 µg of BG505 SOSIP.664 trimer formulated in 75 units of ISCOMATRIX given at week 0, 4, 12, 24,
350 38 and 52. All immunizations and blood samplings were performed at the Wisconsin National
351 Primate Research Center as described previously [24].

352 **Rhesus macaque naïve B-cell repertoire sequencing**

353 Frozen PBMCs from five naïve Indian origin RMs were obtained from Yerkes National Primate
354 Research Center (IACUC approval YER2001036). The cells were rapidly thawed in a 37°C water
355 bath and immediately diluted into 10 mL of pre-warmed RPMI media with 10% (v/v) heat-
356 inactivated fetal bovine serum (FBS). Cells were pelleted at 400xg for 7 minutes and resuspended
357 in 0.5 mL FACS buffer (PBS + 1% (v/v) FBS and stained on ice for 1 hr with the panel of fluorescent
358 antibodies against IgM ([clone G20-127] BD), CD4 ([clone OKT-4] BioLegend), CD3 ([clone SP34-
359 2] BD), IgG ([clone G18-145] BD), CD20 ([clone 2H7] BioLegend), CD8 ([clone RPA-T8] BioLegend),
360 CD14 ([clone M5E2] BD), CD16 ([clone eBioCB16] ThermoFisher) and an eFluor780 viability
361 marker (ThermoFisher). A MoFlo Astrios cell sorter (Beckman Coulter), with gating for live
362 $IgM^+/CD20^+/CD3^-/CD4^-/CD8^-/CD14^-/CD16^-$ cells, was used to isolate cells that were then pelleted
363 at 600xg for 10 min, resuspended in RLT+BME buffer (Qiagen), snap frozen in a dry ice ethanol
364 bath and stored at -80°C. RNA extraction was performed using RNeasy Protect Mini kit (Qiagen)
365 following the manufacturer's instructions. The 5' rapid amplification of cDNA ends (5'RACE) with
366 template switching method was used to obtain cDNA with unique molecular identifiers (UMIs)
367 using a protocol modified from Turchaninova *et al.* [53]. Briefly, 300 ng of RNA was used in a 5'RACE

368 cDNA synthesis reaction. The first-strand cDNA synthesis was performed at 42°C for 1 hr using
369 the RM IgM outer reverse primer (5'-GTGATGGAGTCGGGAAGGAAG-3'), a template switch
370 adaptor with incorporated UMIs (5'-
371 AAGCAGUGGTAUCAACGCAGAGUNNNNUNNNNUNNNNUCTTrGrGrGrG-3'), and SMARTScribe
372 Reverse Transcriptase (Clontech). Residual template switch adaptor was removed by incubation
373 with 5 U of uracil DNA glycosylase (New England BioLabs) for 40 min at 37°C. The resulting cDNA
374 was purified using the MinElute PCR Purification Kit (Qiagen) following the manufacturer's
375 instructions. PCR amplification was performed using the Q5® High-Fidelity DNA Polymerase (New
376 England BioLabs), the forward primer (5'-NNNNAAGCAGTGGTATCAACGCA-3'), and the RM IgM
377 inner reverse primer (5'-NNNNNAGGGGGAAAAGGGTTG-3'). Illumina adaptors were added using
378 the NEBNext® Ultra™ II DNA Library Prep Kit (New England BioLabs) following the manufacturer's
379 instructions. Libraries were sequenced on an Illumina MiSeq using the Illumina v3, (2x 300 bp)
380 sequencing kit.

381 **Indian origin RM germline BCR database**

382 Gene/alleles published by Vigdorovich *et al*. [28] were aligned to the Mmul_8.0.1 Indian origin RM
383 genome assembly using BLAST [29,30]. Sequences that were not identical to the reference genome
384 were eliminated. Additional full-length genes/alleles from available Indian origin RM genomic
385 DNA sequencing datasets [21,31] were added to the database. Duplicates and sequences containing
386 ambiguous bases were removed. The resulting initial Indian origin RM germline BCR database
387 (Table S1) was used for running IgDiscover on additional NGS datasets that were obtained during
388 this study as described above, downloaded from the NCBI SRA [27,34], or obtained directly from the
389 study authors [28]. Paired sequence reads were aligned and filtered for length and quality using

390 VDJServer [54]. Novel germline BCR gene/alleles were inferred using IgDiscover v0.11 with the
391 germline_filter parameters "unique_cdr3s" and "unique_js" set to 10 and 4 respectively to
392 reduce the rate of false positives [27]. Inferred genes/alleles were kept if they were detected in
393 more than one animal or if they were identical to RM genes/alleles that were previously
394 deposited in NCBI. The resulting germline BCR database (available at
395 http://ward.scripps.edu/gld/) was converted into a custom IgBLAST database and subsequently
396 used to analyze the BG505-specific mAb sequences [35].

397 **Env sequence analysis**

398 Prevalence of specific amino acids or potential N-linked glycosylation sites (PNGS) were
399 calculated using HIVAnchor (https://github.com/chazbot72/anchor). Pairwise alignments
400 between the HxB2 Env reference sequence (K03455) and the LANL 2018 Group M super filtered
401 web alignment was performed using Clustal Omega [55]. The results were parsed into a database
402 keyed on positions relative to the reference, with gaps notated as sub positions following the last
403 identical residue. The database was subsequently interrogated for conservation of amino acids
404 or PNGS at specific positions.

405 **Env protein production**

406 BG505 SOSIP.664, BG505 SOSIP.664-D7324 tag, BG505 SOSIP.664-AviTag, BG505 SOSIP.v4.1, and
407 BG505 SOSIP.v5.2 were expressed in HEK293F cells and purified with either PGT145 or 2G12
408 affinity chromatograph followed by size exclusion chromatography (SEC) using a HiLoad® 16/600
409 Superdex® pg200 (GE Healthcare) as described previously [7,8,13]. Monomeric gp120 proteins
410 (AviTag or D7324 tagged) were purified using a *Galanthus nivalis* lectin (Vector Labs) column. The
411 Avi-tagged proteins were biotinylated using the BirA enzyme (Avidity) according to the

412 manufacturer's protocol. The resulting biotinylated proteins are referred to using the descriptor
413 AviB.

414 **Monoclonal antibody isolation**

415 BG505 SOSIP.664-specific IgG^+ memory B-cells from isolated PBMCs from RMs rh1987 and
416 rh2011 were single cell sorted in lysis buffer in order to amplify the antigen-specific mAbs, as
417 previously described [56]. PBMCs were stained with primary fluorophore-conjugated antibodies to
418 human CD3, CD8, CD14, CD20, IgG and IgM (BD Pharmigen). For staining with Env proteins, 50
419 nM of BG505 SOSIP.664-AviB, BG505 SOSIP.664 7C3-AviB or gp120-AviB were coupled in
420 equimolar ratios to Streptavidin-PE, Streptavidin-FITC or Streptavidin-APC (Life Technologies),
421 respectively. Cells were stained for 1 hr at 4°C in PBS supplemented with 1 mM EDTA and 1% FBS.
422 In the gating strategy, we first excluded unwanted cell populations ($CD3^-/CD8^-/CD14^-$) followed
423 by selection of HIV Env-specific (positive for any of the 3 probes) memory B-cells
424 ($CD20^+/IgG^+/IgM^-/HIV^+$). Cells of interest were single-cell sorted using a BD FACSAria III machine,
425 into 96-well plates containing lysis buffer, and immediately stored at -80°C. One round of reverse-
426 transcription and two rounds of nested PCR were performed to amplify the antibody V(D)J genes
427 as previously described by Tiller *et al.*[15]. The PCR products containing the variable regions of the
428 heavy chain or light chain, kappa or lambda were cloned into human IgG expression vectors to
429 produce mAbs as described previously [56]. Fab expression vectors were made by introducing two
430 stop codons following residue D234 (Kabat numbering [57]) in the IgG heavy chain vectors using
431 the QuikChange® Lightning Site-Directed Mutagenesis kit (Agilent). Sequences were verified by
432 Sanger sequencing (Genewiz).

433 **Monoclonal antibody and Fab production**

434 MAbs and Fabs were expressed in HEK293F cells and purified using affinity chromatography.
435 Briefly, HEK293F cells (Invitrogen) were co-transfected with heavy and light chain plasmids (1:1
436 ratio) using PEImax. Transfections were performed according to the manufacturer's protocol.
437 Supernatants were harvested 4-6 days following transfection and passed through a 0.45 µm filter.
438 MAbs were purified using Protein A/G (ThermoFisher) or MAbSelect™ (GE Healthcare) affinity
439 chromatography. Fabs were purified using CaptureSelect™ CH1-XL (ThermoFisher) affinity
440 chromatography.

441 **D7324-capture ELISA for monomeric and trimeric BG505 Env proteins**

442 Binding ELISAs were conducted as described previously [13,40].

443 **TZM-bl cell-based neutralization assays**

444 Neutralization assays using the autologous BG505.T332N virus and mutants, and the
445 heterologous SF162 virus, were carried out as described previously [58]. Nonlinear regression
446 curves were determined and 50% inhibitory concentration (IC_{50}) values were calculated using a
447 sigmoid function in Graphpad Prism v7.03.

448 **Bio-Layer Interferometry (BLI)**

449 An Octet RED instrument (FortéBio) was used to determine the kinetic parameters of the
450 antibody–antigen interactions by Biolayer Interferometry. Monoclonal Fabs were loaded onto
451 anti-human Fab-CH1 (FAB2G) biosensors (FortéBio) at a concentration of 10 µg/mL in kinetics
452 buffer (PBS, pH 7.4, 0.01% [w/v] BSA, and 0.002% [v/v] Tween 20) until a response of 1 nanometer
453 shift was reached. Loaded biosensors were dipped into kinetics buffer for 1 min to acquire a
454 baseline and then moved to wells containing a series of 2-fold dilutions of BG505 SOSIP.v5.2 in
455 kinetics buffer, starting at a 4000 nM. The trimers were allowed to associate for 180 secs before

456 the biosensor were move back to the wells containing kinetics buffer where the baseline was
457 acquired. Disassociation of the trimers from the Fab-loaded biosensors was recorded for 300
458 secs. All BLI experiments were conducted at 37°C. Kinetic parameters were calculated using the
459 Octet System Data Analysis v9.0 (FortéBio).

460 **Negative Stain Electron Microscopy**

461 BG505 SOSIP/Fab complexes were made by mixing 10-15 µg SOSIP with a 3 to 6-fold per protomer
462 molar excess for monoclonal Fabs or 500 µg polyclonal Fabs and allowed to incubate for 18 to 24
463 hrs at room temperature (RT). Complex samples were either diluted to 0.02 mg/mL and applied
464 to glow discharged negative stain grids or they were SEC purified using a Superose™ 6 Increase
465 10/300 GL (GE Healthcare) column to remove excess Fab prior to EM grid preparation. Fractions
466 containing the SOSIP/Fab complexes were pooled and concentrated using 10 kDa Amicon® spin
467 concentrators (Millipore). Samples were diluted to 0.03 mg/mL in TBS (0.05 M Tris pH 7.4, 0.15
468 M NaCl) and adsorbed onto glow discharged carbon-coated Cu400 EM grids (Electron Microscopy
469 Sciences) and blotted after 10 seconds. The grids were then stained with 3 µL of 2% (w/v) uranyl
470 formate, immediately blotted, and stained again for 45 secs followed by a final blot. Image
471 collection and data processing was performed as described previously on either an FEI Tecnai T12
472 microscope (2.05 Å/pixel; 52,000× magnification) or FEI Talos microscope (1.98 Å/pixel; 72,000×
473 magnification) with an electron dose of ~25 electrons/Å^2 using Leginon [59,60]. 2D classification, 3D
474 sorting and 3D refinement conducted using Relion v3.0 [61]. EM density maps were visualized using
475 UCSF Chimera and segmented using Segger [62,63].

476 **X-ray Crystallography Data Collection and Processing**

477 All crystals were grown using sitting drop vapor diffusion. The RM20F Fab was crystallized from
478 a solution containing 10 mg/mL protein in TBS with a well solution containing 0.1M MES, pH 5.0
479 and 2M ammonium sulfate. The crystals were cryoprotected by soaking in a well solution
480 supplemented with 30% ethylene glycol. The RM20J Fab was crystallized from a solution
481 containing 10 mg/mL protein in TBS with a well solution containing 0.1M MES, pH 6.0, 5%
482 PEG3000 and 40% PEG400, with no cryoprotectant supplemented. The RM20E1 Fab was
483 crystallized from a solution containing 6.3 mg/mL protein in TBS with a well solution containing
484 0.1M glycine, pH 10.5, 1.2M NaH_2PO_4, 0.8M Na_2HPO_4, and 0.2M Li_2SO_4, with 15% ethylene glycol
485 supplemented as cryoprotectant. All crystals were grown at 298 K. Diffraction data for RM20F
486 and RM20E1 were collected at the Stanford Synchrotron Radiation Lightsource (SSRL) beamline
487 BL12−2, and that for RM20J collected at the Advanced Photon Source (APS) beamline 23ID-B.
488 Data collection and processing statistics are detailed in Table S5. Data sets were indexed,
489 integrated, and scaled using the HKL-2000 package [64]. The structures were solved by molecular
490 replacement using PHASER [65] with a homology model (SWISS-MODEL; [66-68]) as a search model
491 and further refined using phenix.refine [69] combined with manual building cycles in Coot [70].

492 **Cryo Electron Microscopy Sample Preparation**

493 RM20J complex: 500 µg BG505 SOSIP.v5.2 was mixed with 656 µg RM20J Fab and incubated at
494 RT overnight. The complex was SEC purified using a HiLoad® 16/600 Superdex® pg200 (GE
495 Healthcare) column in TBS. Fractions containing the complex were concentrated to 6.1 mg/mL
496 using a 10 kDa Amicon® spin concentrator (Millipore). 3.5 µL of the complex was mixed with 0.57
497 µL of 0.04 mM lauryl maltose neopentyl glycol (LMNG) and applied to a C-Flat grid (CF-2/1-4C,
498 Protochips, Inc.), which had been plasma-cleaned for 5 seconds using a mixture of N_2/O_2 (Gatan

499 Solarus 950 Plasma system). The grid was blotted and plunged into liquid ethane using a Vitrobot
500 Mark IV (ThermoFisher).
501 RM20F complex: 500 µg BG505 SOSIP.v4.1 was mixed with approximately 1,000 µg RM20F Fab
502 and incubated at RT overnight. The complex was SEC purified using a Superose™ 6 Increase
503 10/300 GL (GE Healthcare) column in TBS. Fractions containing the complex were concentrated
504 to 6 mg/mL using a 10 kDa Amicon® spin concentrator (Millipore). 3 µL of the complex was mixed
505 with 1 µL of a n-Dodecyl-β-D-Maltopyranoside (DDM) solution to a final DDM concentration of
506 0.06 mM and applied to a C-Flat grid (CF-2/2-4C, Protochips, Inc.), which had been plasma-
507 cleaned for 5 seconds using a mixture of N_2/O_2 (Gatan Solarus 950 Plasma system). The grid was
508 blotted and plunged into liquid Ethane using a Vitrobot Mark IV (ThermoFisher).
509 RM20E1 complex: 355 µg BG505 SOSIP.v5.2 was mixed with 484 µg RM20E1 Fab and 484 µg
510 PGT122 Fab and incubated at RT overnight. The complex was SEC purified using a HiLoad® 16/600
511 Superdex® pg200 (GE Healthcare) column in TBS. Fractions containing the complex were
512 concentrated to 4 mg/mL using a 10 kDa Amicon® spin concentrator (Millipore). 3 µL of the
513 complex was mixed with 1 µL of a n-Dodecyl-β-D-Maltopyranoside (DDM) solution to a final DDM
514 concentration of 0.06 mM and applied to a grid (Quantifoil R 1.2/1.3, 400), which had been
515 plasma-cleaned for 5 seconds using a mixture of N_2/O_2 (Gatan Solarus 950 Plasma system). The
516 grid was blotted and plunged into liquid Ethane using a Vitrobot Mark IV (ThermoFisher).
517 **Cryo Electron Microscopy Data Collection and Processing**
518 Samples were imaged on either FEI Titan Krios electron microscope (ThermoFisher) operating at
519 300 keV (RM20F dataset) or a FEI Talos Arctica electron microscope (ThermoFisher) operating at
520 200 keV (RM20J and RM20E1 datasets). Both microscopes were equipped with Gatan K2 Summit

521 direct electron directors operating in counting mode. Automated data collection was performed
522 using the Leginon software suite [59]. Micrograph movie frames were aligned and dose-weighted
523 using MotionCor2 [71], and CTF models were determined using Gctf [72]. Particle picking, 2D
524 classification, Ab-initio reconstruction, and 3D refinement were conducted using cryoSPARCv2 [73].
525 Data collection and processing parameters are reported in Table S4.
526 Initial molecular models of the BG505 SOSIP trimer/Fab complexes were built by docking the Env
527 portion of PDB: 5V8M [74] into the EM density maps along with the relevant Fab crystal structures
528 (PDB: 4JY5 was used for PGT122 [75]) using UCSF Chimera [62]. The Fab constant regions were
529 removed due to flexibility in the elbow region as commonly found in Fab structures [76], the
530 appropriate stabilizing mutations (v4.1 or v5.2) were introduced into the Env sequence, and N-
531 linked glycans were added using Coot [77]. The models were iteratively refined into the EM density
532 maps using RosettaRelax and Coot [70,77-80]. Glycan structures were validated using Privateer [81].
533 Overall structures were evaluated using EMRinger [82] and MolProbity [83]. Protein interface
534 calculations were performed using jsPISA [84]. Final model statistics are summarized in Table S4.

535 **Statistical analysis**

536 Statistical models inherent to Relion 3.0 [61] and cryoSPARC [73] were employed in image analysis to
537 derive 2D classes and 3D models. All ELISA and neutralization assays were conducted with at least
538 duplicate measurements.

539 **Data and Software Availability**

540 The accession numbers for Env-specific BCR sequences are DDBJ/ENA/GenBank: MT002976-
541 MT002992 and MT008262-MT008328. RM IgM BCR sequences are available under BioProject ID:
542 PRJNA604386. Atomic coordinates and structure factors of the reported crystal structure have

543 been deposited in the Protein Data Bank (PDB: 6VOS, 6VOR, 6VSR). Cryo-EM reconstructions have
544 been deposited in the Electron Microscopy Data Bank (EMDB: EMD-21246, EMD-21257, EMD-
545 21232), and in the Protein Data Bank (PDB: 6VN0, 6VO1, 6VLR). The accession numbers for the
546 negative stain 3D EM reconstructions are Electron Microscopy DataBank: EMD-21053, EMD-
547 21055, EMD-21056, EMD-21057, EMD-21058, EMD-21059, EMD-21061, EMD-21062, EMD-
548 21064, EMD-21065, EMD-21066, EMD-21075, EMD-21076, EMD-21077, EMD-21078, EMD-
549 21079, EMD-21080, EMD-21081, EMD-21082, EMD-21083, EMD-21084, EMD-21085, EMD-
550 21086, EMD-21087, EMD-21088, EMD-21089, EMD-21090, EMD-21091, EMD-21092, EMD-
551 21093, EMD-21272, EMD-21273, EMD-21274, EMD-21275, EMD-21276, EMD-21277, EMD-
552 21278.
553
554 **Figure Legends**
555 **Figure 1.** MAb isolation and characterization from BG505 SOSIP.664 trimer-immunized RMs. (A)
556 Simplified immunization scheme adapted from Sanders et al. 2015 [24]. Black arrows indicate i.m.
557 immunizations with 100 µg of BG505 SOSIP.664 with 75 units of ISCOMATRIX adjuvant. Red
558 arrows indicate blood draws. (B) Heavy and light chain genetic characteristics for mAbs isolated
559 from rh1987 and rh2011. (C) TZM-bl neutralization of BG505.T332N, BG505.T332N.N611A, and
560 SF162 pseudoviruses for mAbs isolated from RM rh1987. (D) TZM-bl neutralization of
561 BG505.T332N, BG505.T332N.N611A, and SF162 pseudoviruses for mAbs isolated from RM
562 rh2011. Assay limit of detection was at an IC_{50} of 50 µg/mL.
563 **Figure 2.** Epitope mapping by negative stain electron microscopy. (A) Representative base-
564 targeting mAbs for animals rh1987 and rh2011. (B) Overlapping gp120/gp41 interface epitope

565 targeted by mAbs from both animals. (C) Overlapping FP epitope targeted by mAbs from both
566 animals. (D) Overlapping N289-glycan hole epitope targeted by mAbs from both animals. (E)
567 EMPEM analysis for wk28 IgG from rh2011 and rh1987. All structural figures were generated with
568 UCSF Chimera [62]. EM density maps were segmented with the Segger extension in UCSF Chimera
569 [62,63].

570 **Figure 3.** RM20J binds to the N289 glycan hole region of BG505 SOSIP.v5.2 (A) Segmented 3.9 Å
571 cryoEM reconstruction of RM20J Fab (pink) in complex with BG505 SOSIP.v5.2 (gp120, dark blue;
572 gp41, light blue). (B) and (C) Zoomed-in views of the epitope/paratope interaction between
573 gp120 (blue, ribbon diagram) and RM20J Fab (surface representation). (D) and (E) Comparison of
574 the RM20J epitope with that of the BG505 SOSIP.664 elicited rabbit neutralizing NAb 10A (PDB:
575 6DID) [19,36].

576 **Figure 4.** RM20F binds to a quaternary epitope at the gp120/gp41 interface of BG505 SOSIP.v4.1.
577 (A) Segmented 4.3 Å cryoEM reconstruction of RM20F Fab (orange) in complex with BG505 SOSIP
578 (gp120, dark blue; gp41, light blue). (B) and (C) Zoomed-in views of the epitope/paratope
579 interaction between BG505 SOSIP (gp120, dark blue; gp41s, light blue and light green; ribbon
580 diagram) and RM20F Fab (surface representation). (D) Neutralization data for BG505 mutant
581 pseudoviruses against VRC01, RM20F, and VRC34.

582 **Figure 5.** RM20E1 binds to the fusion peptide of BG505 SOSIP.v5.2. (A) Segmented 4.2 Å cryoEM
583 reconstruction of RM20E1 Fab (yellow) and PGT122 Fab (light green) in complex with BG505
584 SOSIP (gp120, dark blue; gp41, light blue). (B) and (C) Zoomed-in views of the epitope/paratope
585 interaction between BG505 SOSIP (gp120, dark blue; gp41s, light blue and light green; ribbon

586 diagram) and RM20E1 Fab (surface representation). (D) Comparison of RM20E1 and RM20F
587 epitopes to those of FP targeting bNAbs VRC34, ACS202, and DFPH-a.15 [9,25,39,40].
588 **Table S1.** Initial germline BCR database used in IgDiscover
589
590 **Acknowledgements**
591 We thank Jean-Christophe Ducom, Hannah Turner, and Bill Anderson for assistance with
592 computational resources, microscope management, and data collection. We thank Alan Saluk,
593 Brian Seegers, Steven Head, Jessica Ledesma, Curt Wittenberg, and Nitya Bhaskaran for
594 assistance with naïve B-cell sorting and NGS sequencing. This work was supported by the HIV
595 Vaccine Research and Design (HIVRAD) program (P01 AI110657) (A.B.W., R.W.S, J.P.M., and
596 I.A.W.), NIH CHAVI-ID (UM1 AI100663) and CHAVD (UM1 AI44462) awards (A.B.W., I.A.W. and
597 D.R.B.), NIH R01 AI13082 (J.P.M.), the International AIDS Vaccine Initiative Neutralizing Antibody
598 Center, the Bill and Melinda Gates Foundation CAVD (OPP1115782, OPP1132237, OPP1084519,
599 OPP119635), and the European Union's Horizon 2020 research and innovation program under
600 grant agreement no. 681137 (R.W.S.). C.A.C. is supported by the NIH F31 Ruth L. Kirschstein
601 Predoctoral Award Al131873 and by the Achievement Rewards for College Scientists Foundation.
602 R.W.S. is a recipient of a Vici fellowship from the Netherlands Organization for Scientific Research
603 (NWO). G.O. and M.J.v.G. are supported by amfAR Mathilde Krim Fellowships in Basic Biomedical
604 Research grant numbers 109718-63-RKNT and 109514-61-RKVA, respectively. J.v.S. is a recipient
605 of a 2017 AMC Ph.D. Scholarship. Computational analyses of EM data were performed using
606 shared instrumentation funded by NIH grant S10OD021634. Naïve B-cell sorting and NGS
607 sequencing was conducted as part of the Technologies Across Scale graduate course with support

608 from Skaggs Graduate School of Chemical and Biological Sciences at Scripps Research. Use of the
609 Stanford Synchrotron Radiation Lightsource, SLAC National Accelerator Laboratory, is supported
610 by the U.S. Department of Energy, Office of Science, Office of Basic Energy Sciences under
611 Contract No. DE-AC02-76SF00515. The SSRL Structural Molecular Biology Program is supported
612 by the DOE Office of Biological and Environmental Research, and by the National Institutes of
613 Health, National Institute of General Medical Sciences (including P41GM103393). The contents
614 of this publication are solely the responsibility of the authors and do not necessarily represent
615 the official views of NIGMS, NIAID, or NIH.

616

617 **Author Contributions**

618 C.A.C., J.v.S., M.Y., D.O., I.A.W., R.W.S., A.B.W., and M.J.v.G. designed the experiments. C.A.C.,
619 J.v.S., M.S., R.M., P.v.d.W., M.v.B., J.L.T., R.P., J.C., D.S., C.L., and M.J.v.G. performed the
620 experiments. C.A.C., J.v.S., C.L., D.M., and M.J.v.G. analyzed the data. C.A.C., M.Y., D.O., M.S.,
621 L.M.S., G.O., and B.N. performed the structural studies. C.A.C., C.A.B., J.G., and S.C. developed
622 the macaque germline database. E.G.R., D.G.C., and G.S. provided the macaque PBMC samples.
623 V.V., D.N.S., D.R.B., and J.P.M. provided resources. C.A.C., A.B.W., and M.J.v.G. wrote the
624 manuscript with input from all authors.

625

626 **References**

627 1 UNAIDS. Global HIV & AIDS statistics — 2018 fact sheet. (2019).
628 2 Moldt, B. *et al.* Neutralizing antibody affords comparable protection against vaginal and
629 rectal simian/human immunodeficiency virus challenge in macaques. *Aids* **30**, 1543-
630 1551, doi:10.1097/QAD.0000000000001102 (2016).
631 3 Burton, D. R. & Hangartner, L. Broadly Neutralizing Antibodies to HIV and Their Role in
632 Vaccine Design. *Annual review of immunology* **34**, 635-659, doi:10.1146/annurev-
633 immunol-041015-055515 (2016).

634 4 Pegu, A. *et al.* A Meta-analysis of Passive Immunization Studies Shows that Serum-
635 Neutralizing Antibody Titer Associates with Protection against SHIV Challenge. *Cell Host*
636 *& Microbe* **26**, 336-+, doi:10.1016/j.chom.2019.08.014 (2019).
637 5 Wu, X. HIV Broadly Neutralizing Antibodies: VRC01 and Beyond. *Adv Exp Med Biol* **1075**,
638 53-72, doi:10.1007/978-981-13-0484-2_3 (2018).
639 6 Jardine, J. G. *et al.* HIV-1 broadly neutralizing antibody precursor B cells revealed by
640 germline-targeting immunogen. *Science* **351**, 1458-1463, doi:10.1126/science.aad9195
641 (2016).
642 7 Torrents de la Pena, A. *et al.* Improving the Immunogenicity of Native-like HIV-1
643 Envelope Trimers by Hyperstabilization. *Cell Rep* **20**, 1805-1817,
644 doi:10.1016/j.celrep.2017.07.077 (2017).
645 8 de Taeye, S. W. *et al.* Immunogenicity of Stabilized HIV-1 Envelope Trimers with
646 Reduced Exposure of Non-neutralizing Epitopes. *Cell* **163**, 1702-1715,
647 doi:10.1016/j.cell.2015.11.056 (2015).
648 9 Kong, R. *et al.* Antibody Lineages with Vaccine-Induced Antigen-Binding Hotspots
649 Develop Broad HIV Neutralization. *Cell* **178**, 567-584 e519,
650 doi:10.1016/j.cell.2019.06.030 (2019).
651 10 Escolano, A. *et al.* Immunization expands B cells specific to HIV-1 V3 glycan in mice and
652 macaques. *Nature* **570**, 468-473, doi:10.1038/s41586-019-1250-z (2019).
653 11 Escolano, A. *et al.* Sequential Immunization Elicits Broadly Neutralizing Anti-HIV-1
654 Antibodies in Ig Knockin Mice. *Cell* **166**, 1445-1458 e1412,
655 doi:10.1016/j.cell.2016.07.030 (2016).
656 12 Steichen, J. M. *et al.* HIV Vaccine Design to Target Germline Precursors of Glycan-
657 Dependent Broadly Neutralizing Antibodies. *Immunity* **45**, 483-496,
658 doi:10.1016/j.immuni.2016.08.016 (2016).
659 13 Sanders, R. W. *et al.* A next-generation cleaved, soluble HIV-1 Env trimer, BG505
660 SOSIP.664 gp140, expresses multiple epitopes for broadly neutralizing but not non-
661 neutralizing antibodies. *PLoS pathogens* **9**, e1003618, doi:10.1371/journal.ppat.1003618
662 (2013).
663 14 Julien, J. P. *et al.* Crystal structure of a soluble cleaved HIV-1 envelope trimer. *Science*
664 **342**, 1477-1483, doi:10.1126/science.1245625 (2013).
665 15 Lyumkis, D. *et al.* Cryo-EM structure of a fully glycosylated soluble cleaved HIV-1
666 envelope trimer. *Science* **342**, 1484-1490, doi:10.1126/science.1245627 (2013).
667 16 Pancera, M. *et al.* Structure and immune recognition of trimeric pre-fusion HIV-1 Env.
668 *Nature* **514**, 455-461, doi:10.1038/nature13808 (2014).
669 17 Pauthner, M. *et al.* Elicitation of Robust Tier 2 Neutralizing Antibody Responses in
670 Nonhuman Primates by HIV Envelope Trimer Immunization Using Optimized
671 Approaches. *Immunity* **46**, 1073-1088 e1076, doi:10.1016/j.immuni.2017.05.007 (2017).
672 18 Pauthner, M. G. *et al.* Vaccine-Induced Protection from Homologous Tier 2 SHIV
673 Challenge in Nonhuman Primates Depends on Serum-Neutralizing Antibody Titers.
674 *Immunity* **50**, 241-252 e246, doi:10.1016/j.immuni.2018.11.011 (2019).
675 19 McCoy, L. E. *et al.* Holes in the Glycan Shield of the Native HIV Envelope Are a Target of
676 Trimer-Elicited Neutralizing Antibodies. *Cell Rep* **16**, 2327-2338,
677 doi:10.1016/j.celrep.2016.07.074 (2016).

678 20 Klasse, P. J. *et al.* Epitopes for neutralizing antibodies induced by HIV-1 envelope
679 glycoprotein BG505 SOSIP trimers in rabbits and macaques. *PLoS pathogens* **14**,
680 e1006913, doi:10.1371/journal.ppat.1006913 (2018).
681 21 Cirelli, K. M. *et al.* Slow Delivery Immunization Enhances HIV Neutralizing Antibody and
682 Germinal Center Responses via Modulation of Immunodominance. *Cell*,
683 doi:10.1016/j.cell.2019.04.012 (2019).
684 22 Lei, L. *et al.* The HIV-1 Envelope Glycoprotein C3/V4 Region Defines a Prevalent
685 Neutralization Epitope following Immunization. *Cell Rep* **27**, 586-598 e586,
686 doi:10.1016/j.celrep.2019.03.039 (2019).
687 23 Nogal, B. *et al.* Mapping polyclonal antibody responses in non-human primates
688 vaccinated with HIV Env trimer subunit vaccines. *bioRxiv*, 833715, doi:10.1101/833715
689 (2019).
690 24 Sanders, R. W. *et al.* HIV-1 VACCINES. HIV-1 neutralizing antibodies induced by native-
691 like envelope trimers. *Science* **349**, aac4223, doi:10.1126/science.aac4223 (2015).
692 25 Kong, R. *et al.* Fusion peptide of HIV-1 as a site of vulnerability to neutralizing antibody.
693 *Science* **352**, 828-833, doi:10.1126/science.aae0474 (2016).
694 26 Landais, E. & Moore, P. L. Development of broadly neutralizing antibodies in HIV-1
695 infected elite neutralizers. *Retrovirology* **15**, 61, doi:10.1186/s12977-018-0443-0 (2018).
696 27 Corcoran, M. M. *et al.* Production of individualized V gene databases reveals high levels
697 of immunoglobulin genetic diversity. *Nat Commun* **7**, 13642, doi:10.1038/ncomms13642
698 (2016).
699 28 Vigdorovich, V. *et al.* Repertoire comparison of the B-cell receptor-encoding loci in
700 humans and rhesus macaques by next-generation sequencing. *Clin Transl Immunology*
701 **5**, e93, doi:10.1038/cti.2016.42 (2016).
702 29 Johnson, M. *et al.* NCBI BLAST: a better web interface. *Nucleic Acids Res* **36**, W5-9,
703 doi:10.1093/nar/gkn201 (2008).
704 30 Zimin, A. V. *et al.* A new rhesus macaque assembly and annotation for next-generation
705 sequencing analyses. *Biol Direct* **9**, 20, doi:10.1186/1745-6150-9-20 (2014).
706 31 Ramesh, A. *et al.* Structure and Diversity of the Rhesus Macaque Immunoglobulin Loci
707 through Multiple De Novo Genome Assemblies. *Frontiers in immunology* **8**, 1407,
708 doi:10.3389/fimmu.2017.01407 (2017).
709 32 Ralph, D. K. & Matsen, F. A. I. Per-sample immunoglobulin germline inference from B
710 cell receptor deep sequencing data. *arXiv* (2018).
711 33 Gadala-Maria, D., Yaari, G., Uduman, M. & Kleinstein, S. H. Automated analysis of high-
712 throughput B-cell sequencing data reveals a high frequency of novel immunoglobulin V
713 gene segment alleles. *Proceedings of the National Academy of Sciences of the United*
714 *States of America* **112**, E862-870, doi:10.1073/pnas.1417683112 (2015).
715 34 Guo, K. *et al.* Immunoglobulin VH gene diversity and somatic hypermutation during SIV
716 infection of rhesus macaques. *Immunogenetics* **67**, 355-370, doi:10.1007/s00251-015-
717 0844-3 (2015).
718 35 Ye, J., Ma, N., Madden, T. L. & Ostell, J. M. IgBLAST: an immunoglobulin variable domain
719 sequence analysis tool. *Nucleic Acids Res* **41**, W34-40, doi:10.1093/nar/gkt382 (2013).

720 36 Bianchi, M. *et al.* Electron-Microscopy-Based Epitope Mapping Defines Specificities of
721 Polyclonal Antibodies Elicited during HIV-1 BG505 Envelope Trimer Immunization.
722 *Immunity* **49**, 288-300 e288, doi:10.1016/j.immuni.2018.07.009 (2018).
723 37 Cao, L. *et al.* Differential processing of HIV envelope glycans on the virus and soluble
724 recombinant trimer. *Nat Commun* **9**, 3693, doi:10.1038/s41467-018-06121-4 (2018).
725 38 Struwe, W. B. *et al.* Site-Specific Glycosylation of Virion-Derived HIV-1 Env Is Mimicked
726 by a Soluble Trimeric Immunogen. *Cell Rep* **24**, 1958-1966 e1955,
727 doi:10.1016/j.celrep.2018.07.080 (2018).
728 39 Yuan, M. *et al.* Conformational Plasticity in the HIV-1 Fusion Peptide Facilitates
729 Recognition by Broadly Neutralizing Antibodies. *Cell Host Microbe* **25**, 873-883 e875,
730 doi:10.1016/j.chom.2019.04.011 (2019).
731 40 van Gils, M. J. *et al.* An HIV-1 antibody from an elite neutralizer implicates the fusion
732 peptide as a site of vulnerability. *Nat Microbiol* **2**, 16199,
733 doi:10.1038/nmicrobiol.2016.199 (2016).
734 41 Dubrovskaya, V. *et al.* Vaccination with Glycan-Modified HIV NFL Envelope Trimer-
735 Liposomes Elicits Broadly Neutralizing Antibodies to Multiple Sites of Vulnerability.
736 *Immunity* **51**, 915-929 e917, doi:10.1016/j.immuni.2019.10.008 (2019).
737 42 Yang, L. *et al.* Structure-Guided Redesign Improves NFL HIV Env Trimer Integrity and
738 Identifies an Inter-Protomer Disulfide Permitting Post-Expression Cleavage. *Frontiers in*
739 *immunology* **9**, 1631, doi:10.3389/fimmu.2018.01631 (2018).
740 43 Cao, L. *et al.* Global site-specific N-glycosylation analysis of HIV envelope glycoprotein.
741 *Nat Commun* **8**, 14954, doi:10.1038/ncomms14954 (2017).
742 44 Xu, K. *et al.* Epitope-based vaccine design yields fusion peptide-directed antibodies that
743 neutralize diverse strains of HIV-1. *Nature medicine* **24**, 857-867, doi:10.1038/s41591-
744 018-0042-6 (2018).
745 45 Cheng, C. *et al.* Consistent elicitation of cross-clade HIV-neutralizing responses achieved
746 in guinea pigs after fusion peptide priming by repetitive envelope trimer boosting. *PloS*
747 *one* **14**, e0215163, doi:10.1371/journal.pone.0215163 (2019).
748 46 Brouwer, P. J. M. *et al.* Enhancing and shaping the immunogenicity of native-like HIV-1
749 envelope trimers with a two-component protein nanoparticle. *Nat Commun* **10**, 4272,
750 doi:10.1038/s41467-019-12080-1 (2019).
751 47 Kulp, D. W. *et al.* Structure-based design of native-like HIV-1 envelope trimers to silence
752 non-neutralizing epitopes and eliminate CD4 binding. *Nat Commun* **8**, 1655,
753 doi:10.1038/s41467-017-01549-6 (2017).
754 48 Georgiev, I. S. *et al.* Two-Component Ferritin Nanoparticles for Multimerization of
755 Diverse Trimeric Antigens. *ACS Infect Dis* **4**, 788-796, doi:10.1021/acsinfecdis.7b00192
756 (2018).
757 49 Ringe, R. P. *et al.* Neutralizing antibody induction by HIV-1 Envelope glycoprotein SOSIP
758 trimers on iron oxide nanoparticles may be impaired by mannose binding lectin. *J Virol*,
759 doi:10.1128/JVI.01883-19 (2019).
760 50 Wang, Y. *et al.* HIV-1 Cross-Reactive Primary Virus Neutralizing Antibody Response
761 Elicited by Immunization in Nonhuman Primates. *J Virol* **91**, doi:10.1128/JVI.00910-17
762 (2017).

763 51 Martinez-Murillo, P. *et al.* Particulate Array of Well-Ordered HIV Clade C Env Trimers
764 Elicits Neutralizing Antibodies that Display a Unique V2 Cap Approach. *Immunity* **46**,
765 804-817 e807, doi:10.1016/j.immuni.2017.04.021 (2017).
766 52 Phad, G. E. *et al.* Extensive dissemination and intraclonal maturation of HIV Env vaccine-
767 induced B cell responses. *The Journal of experimental medicine* **217**,
768 doi:10.1084/jem.20191155 (2020).
769 53 Turchaninova, M. A. *et al.* High-quality full-length immunoglobulin profiling with unique
770 molecular barcoding. *Nature protocols* **11**, 1599-1616, doi:10.1038/nprot.2016.093
771 (2016).
772 54 Christley, S. *et al.* VDJServer: A Cloud-Based Analysis Portal and Data Commons for
773 Immune Repertoire Sequences and Rearrangements. *Frontiers in immunology* **9**, 976,
774 doi:10.3389/fimmu.2018.00976 (2018).
775 55 Sievers, F. & Higgins, D. G. Clustal Omega for making accurate alignments of many
776 protein sequences. *Protein science : a publication of the Protein Society* **27**, 135-145,
777 doi:10.1002/pro.3290 (2018).
778 56 Sok, D. *et al.* Recombinant HIV envelope trimer selects for quaternary-dependent
779 antibodies targeting the trimer apex. *Proceedings of the National Academy of Sciences*
780 *of the United States of America* **111**, 17624-17629, doi:10.1073/pnas.1415789111
781 (2014).
782 57 Kabat, E. A. *Sequences of proteins of immunological interest : tabulation and analysis of*
783 *amino acid and nucleic acid sequences of precursors, V-regions, C-regions, J-chain, T-cell*
784 *receptors for antigenm T-cell surface antigens, [beta]2-microglobulins,major*
785 *histocompatibility antigens, Thy-1, complement, C-reactive protein, thymopoietin,*
786 *integrins, post-gamme globulin, [alpha]2-macroglobulins, and other related proteins*. 5th
787 edn, (U.S. Dept. of Health and Human Services, Public Health Service, National Institutes
788 of Health, 1991).
789 58 Derking, R. *et al.* Comprehensive antigenic map of a cleaved soluble HIV-1 envelope
790 trimer. *PLoS pathogens* **11**, e1004767, doi:10.1371/journal.ppat.1004767 (2015).
791 59 Suloway, C. *et al.* Automated molecular microscopy: the new Leginon system. *Journal of*
792 *structural biology* **151**, 41-60, doi:10.1016/j.jsb.2005.03.010 (2005).
793 60 Pugach, P. *et al.* A native-like SOSIP.664 trimer based on an HIV-1 subtype B env gene. *J*
794 *Virol* **89**, 3380-3395, doi:10.1128/JVI.03473-14 (2015).
795 61 Zivanov, J. *et al.* New tools for automated high-resolution cryo-EM structure
796 determination in RELION-3. *eLife* **7**, doi:10.7554/eLife.42166 (2018).
797 62 Pettersen, E. F. *et al.* UCSF Chimera--a visualization system for exploratory research and
798 analysis. *J Comput Chem* **25**, 1605-1612, doi:10.1002/jcc.20084 (2004).
799 63 Pintilie, G. D., Zhang, J., Goddard, T. D., Chiu, W. & Gossard, D. C. Quantitative analysis
800 of cryo-EM density map segmentation by watershed and scale-space filtering, and fitting
801 of structures by alignment to regions. *Journal of structural biology* **170**, 427-438,
802 doi:10.1016/j.jsb.2010.03.007 (2010).
803 64 Otwinowski, Z. & Minor, W. Processing of X-ray diffraction data collected in oscillation
804 mode. *Methods Enzymol* **276**, 307-326 (1997).
805 65 McCoy, A. J. *et al.* Phaser crystallographic software. *J Appl Crystallogr* **40**, 658-674,
806 doi:10.1107/S0021889807021206 (2007).

807 66 Arnold, K., Bordoli, L., Kopp, J. & Schwede, T. The SWISS-MODEL workspace: a web-
808 based environment for protein structure homology modelling. *Bioinformatics* **22**, 195-
809 201, doi:10.1093/bioinformatics/bti770 (2006).
810 67 Biasini, M. *et al.* SWISS-MODEL: modelling protein tertiary and quaternary structure
811 using evolutionary information. *Nucleic Acids Res* **42**, W252-258,
812 doi:10.1093/nar/gku340 (2014).
813 68 Bordoli, L. *et al.* Protein structure homology modeling using SWISS-MODEL workspace.
814 *Nature protocols* **4**, 1-13, doi:10.1038/nprot.2008.197 (2009).
815 69 Adams, P. D. *et al.* PHENIX: a comprehensive Python-based system for macromolecular
816 structure solution. *Acta crystallographica. Section D, Biological crystallography* **66**, 213-
817 221, doi:10.1107/S0907444909052925 (2010).
818 70 Emsley, P., Lohkamp, B., Scott, W. G. & Cowtan, K. Features and development of Coot.
819 *Acta crystallographica. Section D, Biological crystallography* **66**, 486-501,
820 doi:10.1107/S0907444910007493 (2010).
821 71 Zheng, S. Q. *et al.* MotionCor2: anisotropic correction of beam-induced motion for
822 improved cryo-electron microscopy. *Nature methods* **14**, 331-332,
823 doi:10.1038/nmeth.4193 (2017).
824 72 Zhang, K. Gctf: Real-time CTF determination and correction. *Journal of structural biology*
825 **193**, 1-12, doi:10.1016/j.jsb.2015.11.003 (2016).
826 73 Punjani, A., Rubinstein, J. L., Fleet, D. J. & Brubaker, M. A. cryoSPARC: algorithms for
827 rapid unsupervised cryo-EM structure determination. *Nature methods* **14**, 290-296,
828 doi:10.1038/nmeth.4169 (2017).
829 74 Lee, J. H. *et al.* A Broadly Neutralizing Antibody Targets the Dynamic HIV Envelope
830 Trimer Apex via a Long, Rigidified, and Anionic beta-Hairpin Structure. *Immunity* **46**,
831 690-702, doi:10.1016/j.immuni.2017.03.017 (2017).
832 75 Julien, J. P. *et al.* Broadly neutralizing antibody PGT121 allosterically modulates CD4
833 binding via recognition of the HIV-1 gp120 V3 base and multiple surrounding glycans.
834 *PLoS pathogens* **9**, e1003342, doi:10.1371/journal.ppat.1003342 (2013).
835 76 Bailey, L. J. *et al.* Locking the Elbow: Improved Antibody Fab Fragments as Chaperones
836 for Structure Determination. *Journal of molecular biology* **430**, 337-347,
837 doi:10.1016/j.jmb.2017.12.012 (2018).
838 77 van Beusekom, B. *et al.* Building and rebuilding N-glycans in protein structure models.
839 *Acta Crystallogr D Struct Biol* **75**, 416-425, doi:10.1107/S2059798319003875 (2019).
840 78 DiMaio, F., Tyka, M. D., Baker, M. L., Chiu, W. & Baker, D. Refinement of protein
841 structures into low-resolution density maps using rosetta. *Journal of molecular biology*
842 **392**, 181-190, doi:10.1016/j.jmb.2009.07.008 (2009).
843 79 Frenz, B. *et al.* Automatically Fixing Errors in Glycoprotein Structures with Rosetta.
844 *Structure*, doi:10.1016/j.str.2018.09.006 (2018).
845 80 Casanal, A., Lohkamp, B. & Emsley, P. Current Developments in Coot for
846 Macromolecular Model Building of Electron Cryo-microscopy and Crystallographic Data.
847 *Protein science : a publication of the Protein Society*, doi:10.1002/pro.3791 (2019).
848 81 Agirre, J. *et al.* Privateer: software for the conformational validation of carbohydrate
849 structures. *Nature structural & molecular biology* **22**, 833-834, doi:10.1038/nsmb.3115
850 (2015).

851 82 Barad, B. A. *et al.* EMRinger: side chain-directed model and map validation for 3D cryo-
852 electron microscopy. *Nature methods* **12**, 943-946, doi:10.1038/nmeth.3541 (2015).
853 83 Williams, C. J. *et al.* MolProbity: More and better reference data for improved all-atom
854 structure validation. *Protein science : a publication of the Protein Society* **27**, 293-315,
855 doi:10.1002/pro.3330 (2018).
856 84 Krissinel, E. Stock-based detection of protein oligomeric states in jsPISA. *Nucleic Acids*
857 *Res* **43**, W314-319, doi:10.1093/nar/gkv314 (2015).
858

Figure#1

A

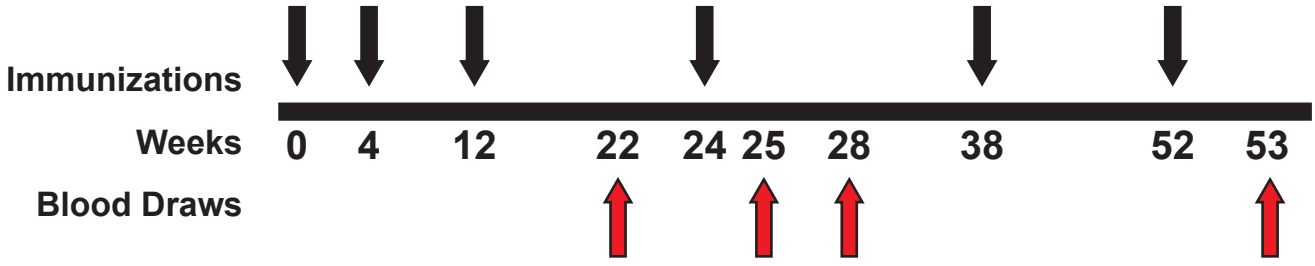

B

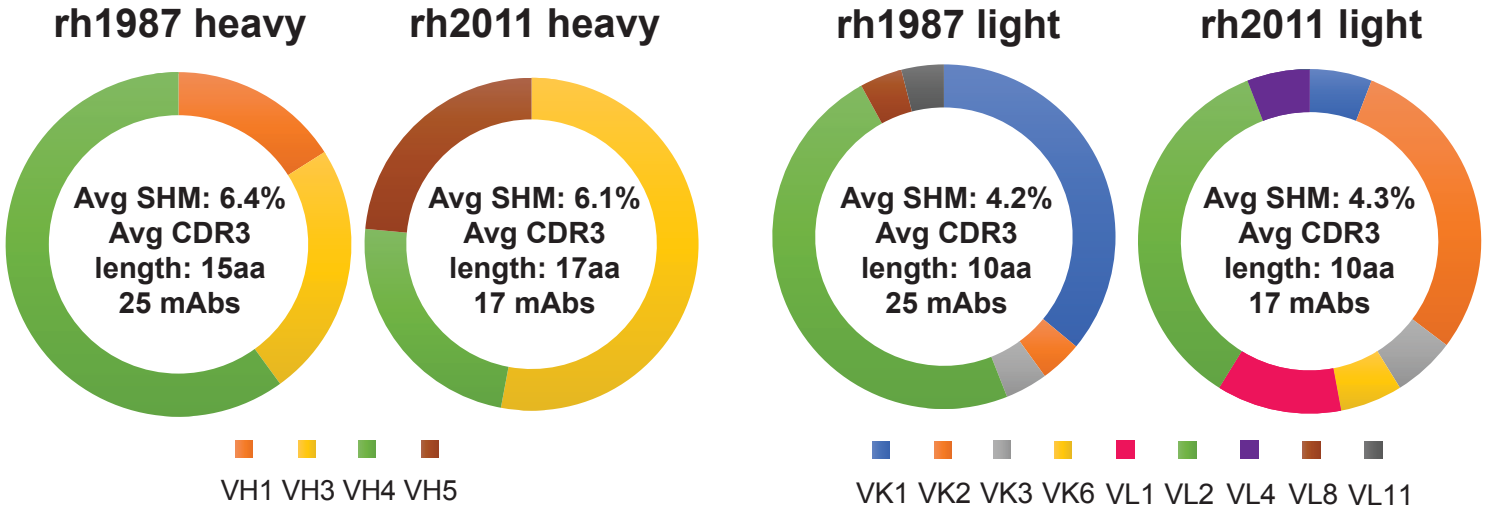

C

rh1987

mAb	BG505 T332N	BG505 T332N+N611A	SF162
RM19A	41.8	>50	>50
RM19A1	44.9	>50	>50
RM19A2	>50	>50	>50
RM19A3	>50	>50	>50
RM19B1	>50	>50	>50
RM19C3	>50	>50	>50
RM19C4	>50	>50	>50
RM19D	>50	>50	>50
RM19J	>50	>50	>50
RM19M	12.9	5.63	>50
RM19N	>50	>50	>50
RM19O	>50	25.5	>50
RM19P	23.5	>50	>50
RM19R	>50	>50	>50
RM19S	>50	3.51	>50
RM19T	>50	>50	>50

IC_{50} (µg/mL)

D

rh2011

mAb	BG505 T332N	BG505 T332N+N611A	SF162
RM20A3	>50	>50	>50
RM20B	>50	>50	>50
RM20C	>50	>50	>50
RM20D	>50	>50	>50
RM20E	>50	<0.41	>50
RM20E1	>50	<0.41	>50
RM20E2	>50	<0.41	>50
RM20E3	>50	<0.41	>50
RM20F	1.6	<0.41	>50
RM20H	42.9	<0.41	>50
RM20I	>50	>50	>50
RM20J	>50	>50	>50

IC_{50} (µg/mL)

Figure#2

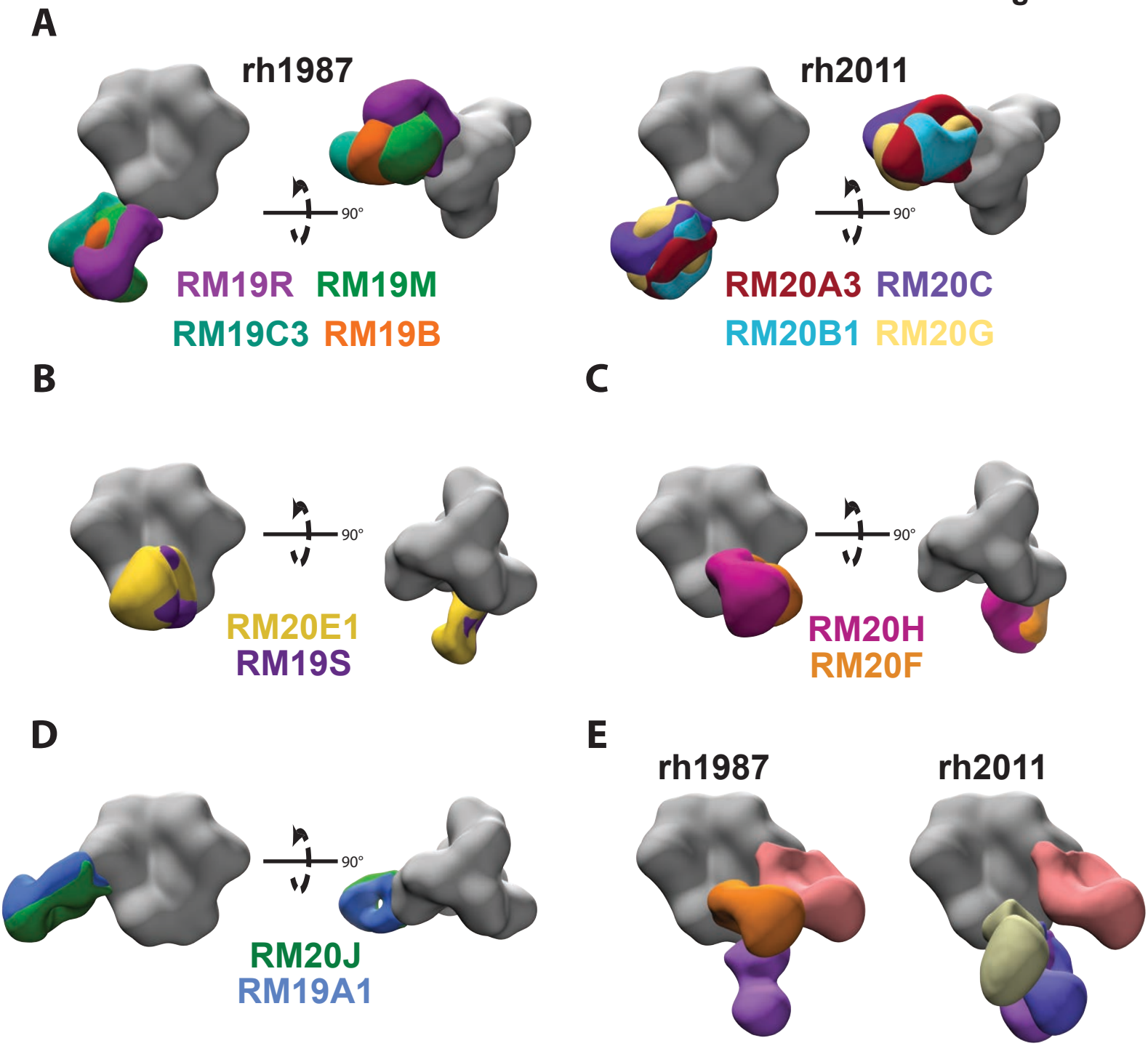
A
rh1987
90°
RM19R
RM19M
RM19C3
RM19B
rh2011
90°
RM20A3
RM20C
RM20B1
RM20G
B
90°
RM20E1
RM19S
C
90°
RM20H
RM20F
D
90°
RM20J
RM19A1
E
rh1987
rh2011

Figure#3

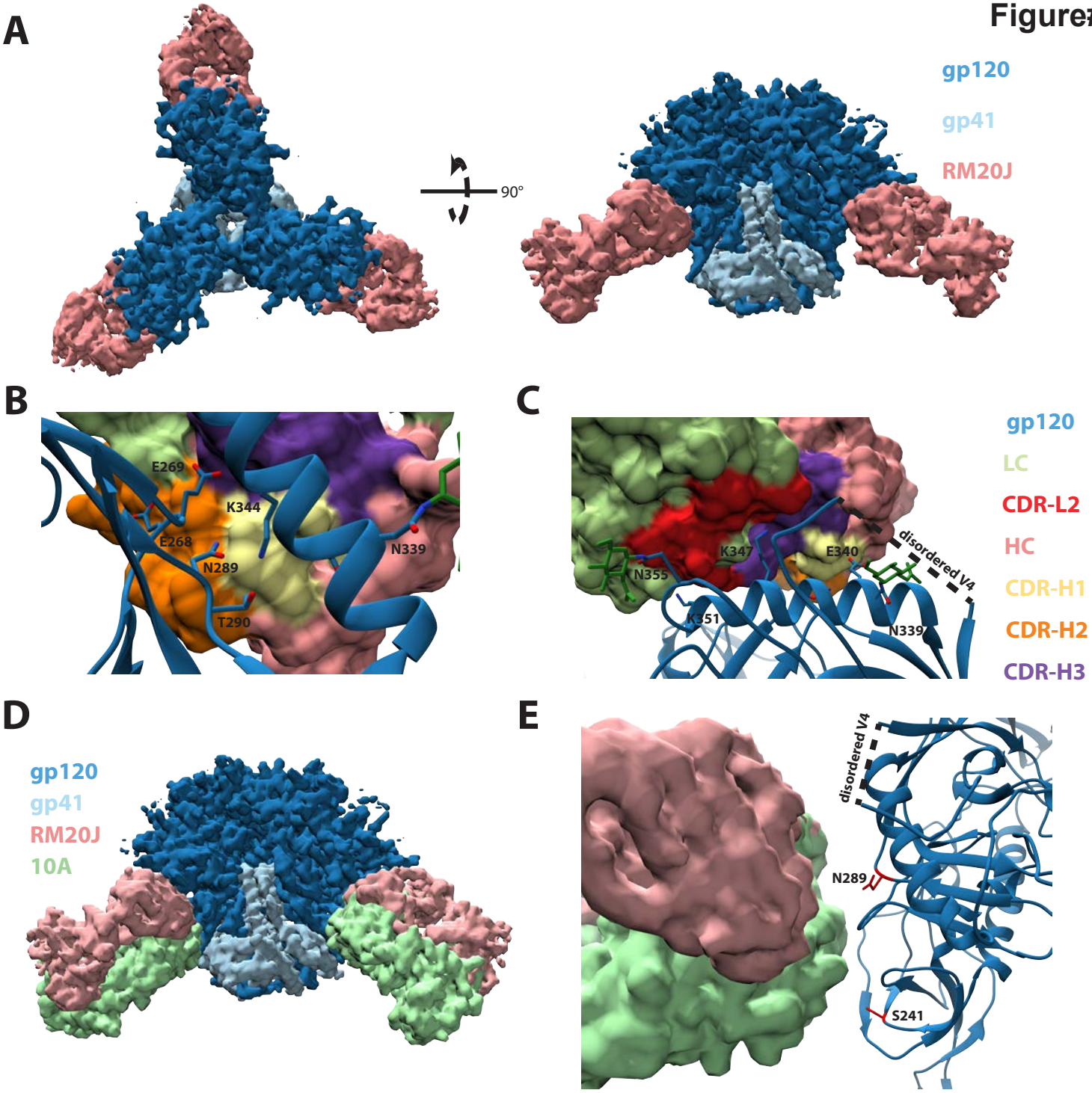
A
gp120
gp41
RM20J
90°
B
E269
K344
E268
N289
T290
N339
C
gp120
LC
CDR-L2
HC
CDR-H1
CDR-H2
CDR-H3
K347
E340
N355
K351
N339
disordered V4
D
gp120
gp41
RM20J
10A
E
disordered V4
N289
S241

Figure#4

A

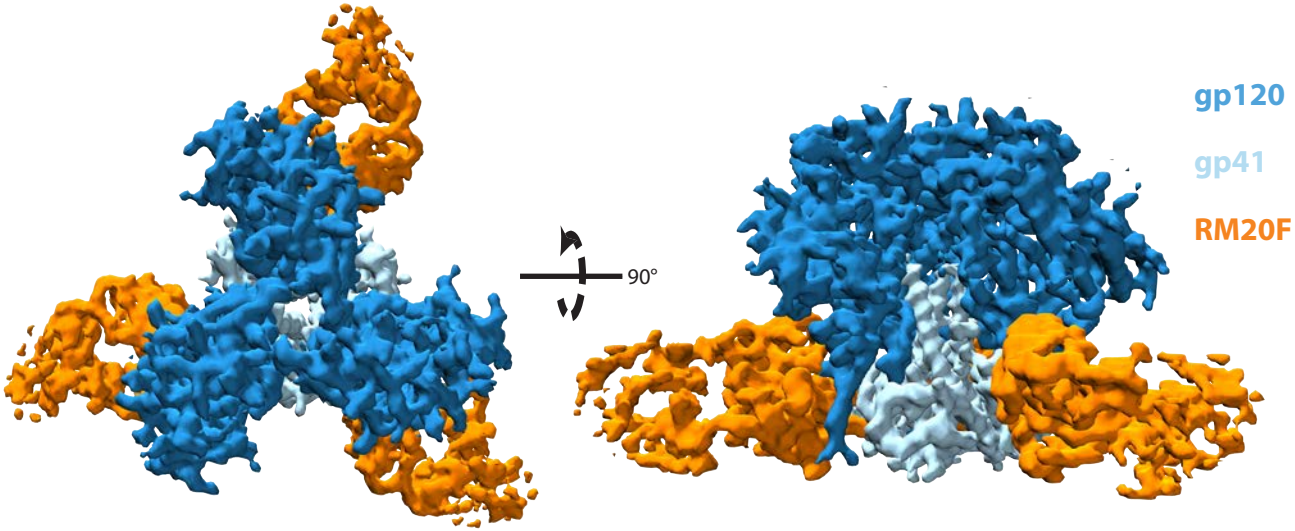

B

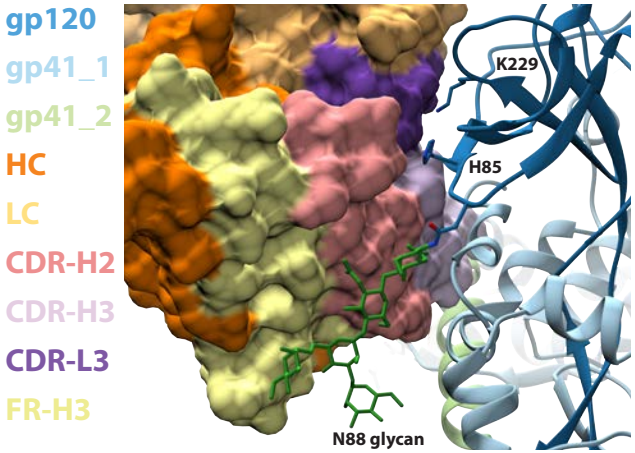

C

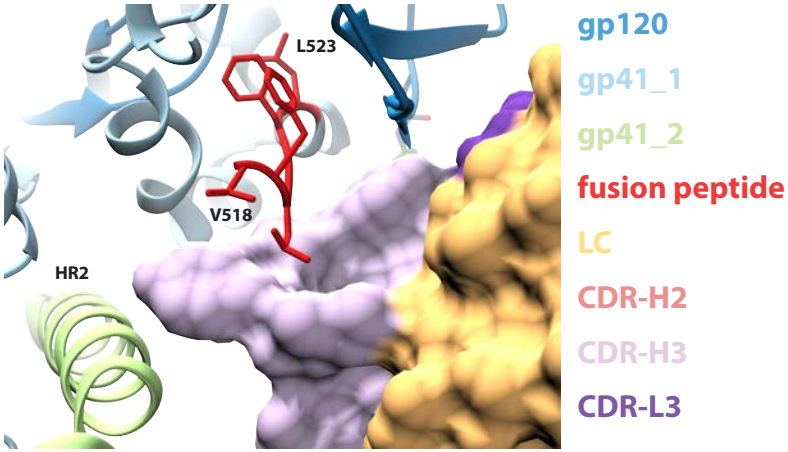

D

	VRC01	RM20F	VRC34
WT	1.0	1.0	1.0
H85A	1.2	11.9	4.7
E87A	1.2	4.3	0.8
N88A	1	>28	>24
K229A	0.6	3.1	1.2
S241N	1.1	6.6	n.d.
E267A	0.8	1.3	0.9
P291T	1.1	2.9	n.d.
N332T	0.9	0.5	n.d.
F522A	0.8	3.9	1.0
M535A	0.9	2.9	1.0
T536A	0.8	2.9	1.5
T538A	0.8	3.6	1.2
N611Q	1.5	<0.1	n.d.
N625Q	1.9	0.6	n.d.
N637Q	1.6	1.2	n.d.
G644A	1.0	4.2	1.8
E647A	1.7	13.5	0.6

fold reduction in neutralization

Figure#5

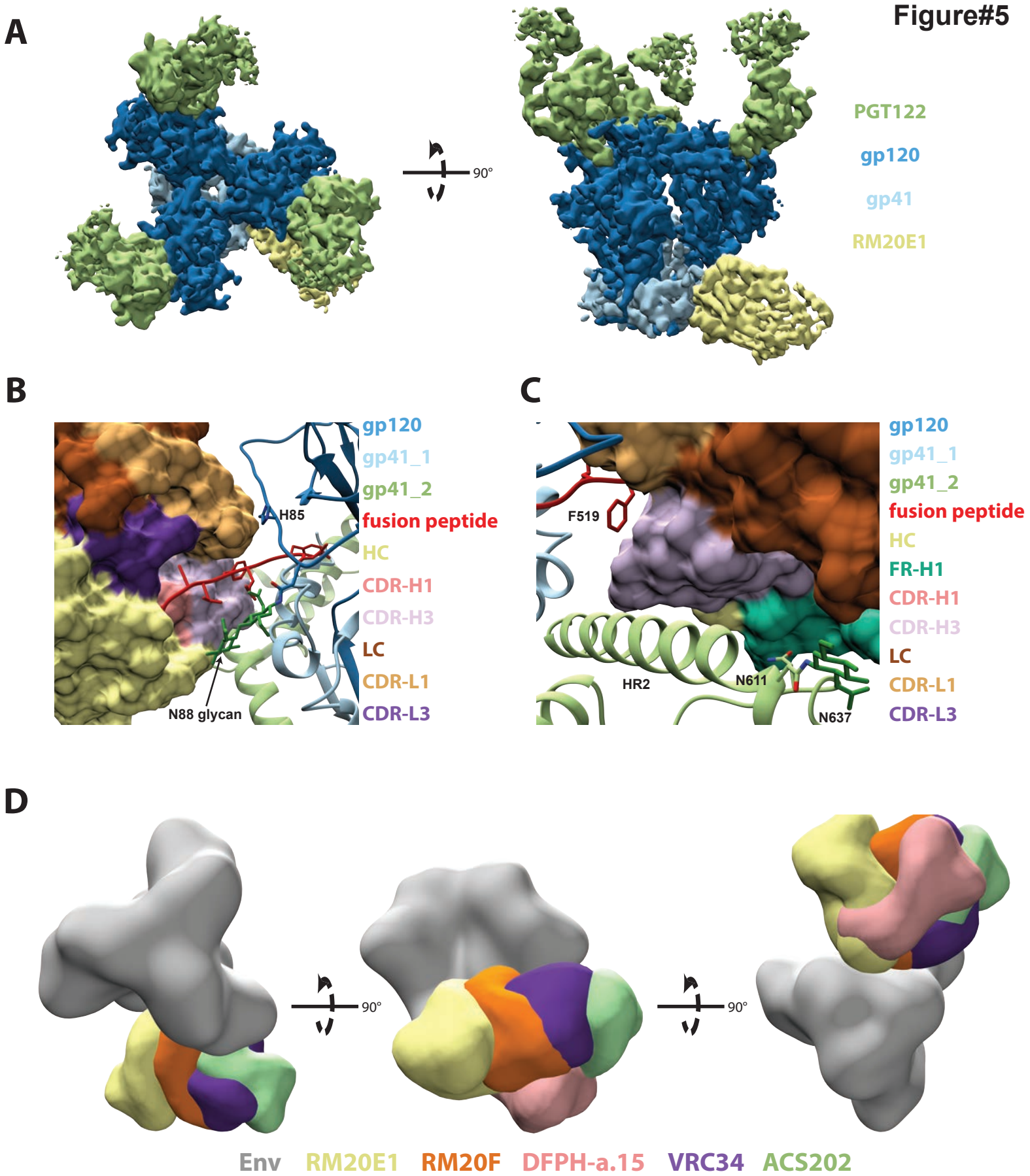
A
90°
PGT122
gp120
gp41
RM20E1
B
gp120
gp41_1
gp41_2
fusion peptide
HC
CDR-H1
CDR-H3
LC
CDR-L1
CDR-L3
H85
N88 glycan
C
gp120
gp41_1
gp41_2
fusion peptide
HC
FR-H1
CDR-H1
CDR-H3
LC
CDR-L1
CDR-L3
F519
HR2
N611
N637
D
90°
90°
Env
RM20E1
RM20F
DFPH-a.15
VRC34
ACS202